AD-A139 189 NONLINEAR INTERACTIONS BETWEEN THE PUMPING KINETICS FLUID DYNAMICS AND OP..(U) ILLINOIS UNIV AT URBANA DEPT OF AERONAUTICAL AND ASTRONAUTICA.. L H SENTMAN ET AL. 1/1

UNCLASSIFIED DEC 83 AAE-83-10 AFOSR-TR-84-0147 F/G 20/5 NL

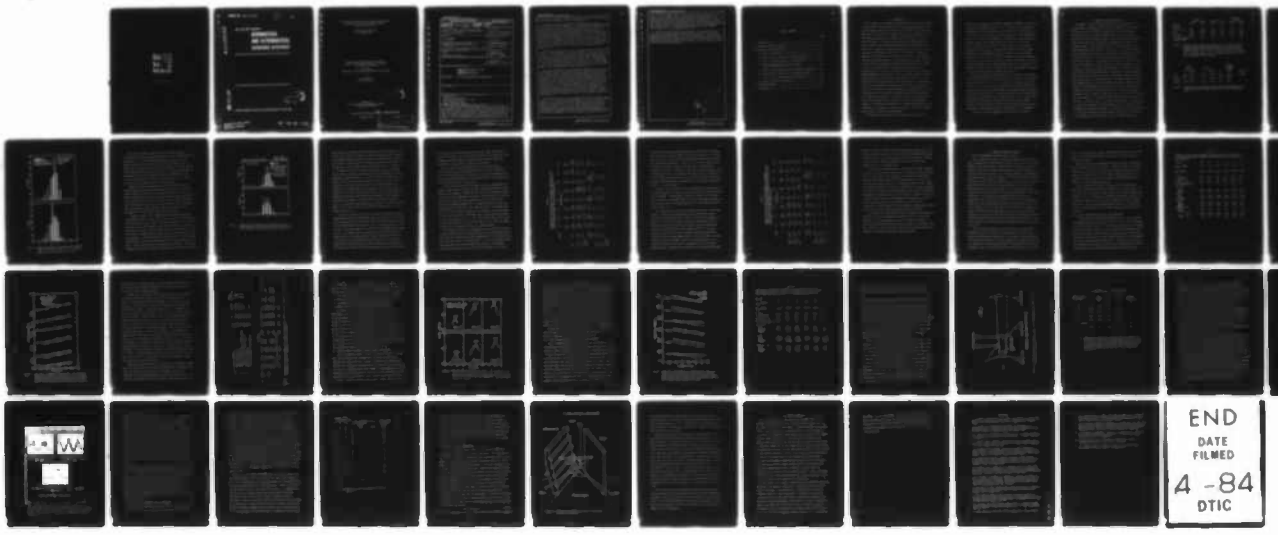

END
DATE FILMED
4 -84
DTIC

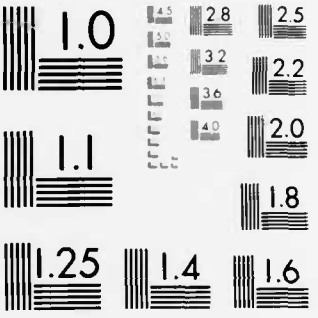

(12)

AAE

AERONAUTICAL AND ASTRONAUTICAL ENGINEERING DEPARTMENT

ENGINEERING EXPERIMENT STATION, COLLEGE OF ENGINEERING, UNIVERSITY OF ILLINOIS, URBANA

Aeronautical and Astronautical Engineering Department
University of Illinois at Urbana-Champaign
Urbana, Illinois 61801

Technical Report AAE 83-10
UILU ENG 83 0510

Nonlinear Interactions Between the Pumping Kinetics, Fluid Dynamics and Optical Resonator of cw Fluid Flow Lasers

L. H. Sentman
Aeronautical and Astronautical Engineering Department

and

M. H. Nayfeh
Physics Department

Prepared for
Air Force Office of Scientific Research
Bolling AFB, DC 20332

Final Report AFOSR Grant ~~80-0133~~ # - AFOSR-80-0133

December, 1983

UNCLASSIFIED
SECURITY CLASSIFICATION OF THIS PAGE (When Data Entered)

i

REPORT DOCUMENTATION PAGE

READ INSTRUCTIONS BEFORE COMPLETING FORM

1. REPORT NUMBER: AFOSR-TR- 84-0147
2. GOVT ACCESSION NO.: A139 189
3. RECIPIENT'S CATALOG NUMBER:

4. TITLE (and Subtitle): Nonlinear Interactions Between the Pumping Kinetics, Fluid Dynamics and Optical Resonator of cw Fluid Flow Lasers

5. TYPE OF REPORT & PERIOD COVERED: Final Report

6. PERFORMING ORG. REPORT NUMBER:

7. AUTHOR(s):
L. H. Sentman
M. H. Nayfeh

8. CONTRACT OR GRANT NUMBER(s): AFOSR-80-0133

9. PERFORMING ORGANIZATION NAME AND ADDRESS:
Aeronautical & Astronautical Engr. Dept.
Physics Dept.
U. of Ill. at Urbana-Champaign, Urbana, IL 61801

10. PROGRAM ELEMENT, PROJECT, TASK AREA & WORK UNIT NUMBERS: 61102F 2303/B1

11. CONTROLLING OFFICE NAME AND ADDRESS:
AFOSR
NC
Bolling AFB, DC 20332

12. REPORT DATE: December 1983

13. NUMBER OF PAGES: 49

14. MONITORING AGENCY NAME & ADDRESS (if different from Controlling Office):

15. SECURITY CLASS. (of this report): UNCLASSIFIED

15a. DECLASSIFICATION DOWNGRADING SCHEDULE:

16. DISTRIBUTION STATEMENT (of this Report):

Approved for public release,
distribution unlimited

17. DISTRIBUTION STATEMENT (of the abstract entered in Block 20, if different from Report):

18. SUPPLEMENTARY NOTES:

19. KEY WORDS (Continue on reverse side if necessary and identify by block number)
Chemical laser
Rotational nonequilibrium
Time dependent pulsations in cw power
Kinetics-Physical optics
Confocal unstable resonator

20. ABSTRACT (Continue on reverse side if necessary and identify by block number)

The theoretical and experimental studies directed toward measuring the amplitude and frequency of the time dependent oscillations in power which have been predicted to occur in cw HF chemical lasers that employ an unstable resonator to extract power are summarized. The MNORO model was generalized to include rotational nonequilibrium in the HF(0) level as well as in HF(1) and HF(2). To obtain the correct power split between vibrational bands, it was necessary to add to the MNORO kinetics model the backward rate for the cold

DD FORM 1 JAN 73 1473

UNCLASSIFIED
SECURITY CLASSIFICATION OF THIS PAGE (When Data Entered)

pumping reaction to HF(3), the HF-H_2 and HF-HF VV reactions and the deactivation of HF by the DF which is formed in the combustor.

A stable resonator model was coupled to the MNORO3 kinetics model to provide a theoretical model (MNORO3SR) for a laser employing a stable resonator. Six of the eight criteria for convergence were satisfied for the Helios CL II test case while two of the eight criteria indicated the solution had not converged. The spectra predicted with the stable resonator model were in better agreement with the data (which was taken with a stable resonator) than were the spectra predicted with the Fabry-Perot model. A study of the effect of the mixing rate showed that the power spectral distribution is significantly affected by the mixing rate. This implies that for situations in which the fluid dynamics of the mixing process are so complicated that they are represented by a very approximate model, the determination of the mixing parameters cannot be considered fixed until a rotational nonequilibrium calculation for the resonator for which the data were taken has shown agreement with the measured spectra.

A physical optics model was coupled to the MNORO3 kinetics model to provide a theoretical model (MNORO3UR) for a laser employing a confocal, unstable resonator. All seven of the convergence criteria were satisfied for the Helios CL II test case. The physical optics-kinetics calculations showed that the time-dependent oscillations which may occur on lines whose saturated gain does not fill the resonator are Fresnel number dependent. For a Fresnel number of 1.5, the time-dependent oscillations did not occur, while, for Fresnel numbers of 18.57 and 9.457, the time-dependent oscillations did occur. For all cases in which the time-dependent oscillations occurred, the period was mostly 40 ns with some lines varying between 33 and 40 or 40 and 47 ns.

The comparison between the laser performance predicted using the new and the old HF rate packages showed that the new rate package gives 43% more total power compared to the old rate package, with over half of this difference in the 2→1 vibrational band, and gives a mode length 99% greater than the old rate package. These differences are the result of the omission of the multiquantum deactivation reactions by HF and F and the collisional decomposition of HF(3) by H from the new rate package. The removal of power from the upper vibrational bands is accomplished by the single quantum and the DF deactivation reactions in the new rate package whereas in the old rate package, the removal of power from the upper vibrational bands is accomplished by the collisional decomposition of HF(v), $v \geq 3$ by H atoms. The MNORO3 rotational nonequilibrium calculations showed that the new rate package gives 35% more total power and 30% longer mode width than the old rate package. However, the spectra given by both rate packages agree well with each other and with the data for the CL XI.

The multi-line performance (power and power spectral distribution) of the Helios CL II cw HF chemical laser was measured as a function of the SF_6 and H_2 flow rates, cavity losses, pressure and resonator type. The very good agreement of the Fabry-Perot, stable resonator and unstable resonator laser models with the data as the flow rates, cavity losses and pressure change verified the models. The major result of this research program was the measurement of the amplitude, frequency and Fresnel number dependence of the time-dependent oscillations which occur on lines whose saturated gain does not fill the unstable resonator. The data showed that the oscillations do not

occur for Fresnel numbers below 1.5 and that their amplitudes increase as the fraction of the resonator filled by the oscillating lines decreased. The measured periods were mostly 40 ns with some lines varying between 33 and 50 ns. The amplitude modulation varied from 12% to 80%. In addition, in some cases there was a 7 ns oscillation superimposed on the 40 ns oscillation, which, based on the mirror spacing, is probably a mode beating. The a priori prediction of these characteristics of the time-dependent oscillations by the MNORO3UR computer model was in good agreement with the data.

Several other new results were also obtained. The first data from a cw laser for a near resonant energy transfer from v=3, J=3,4 to v=2, J=14 with a subsequent rotational cascade to v=2, J=11 were obtained. In addition, the stable resonator data indicated that the polarization introduced by the Brewster windows affects the power spectral distribution. Preliminary data with a new He injector indicated that under certain conditions, it was possible to obtain a 60% increase in laser performance.

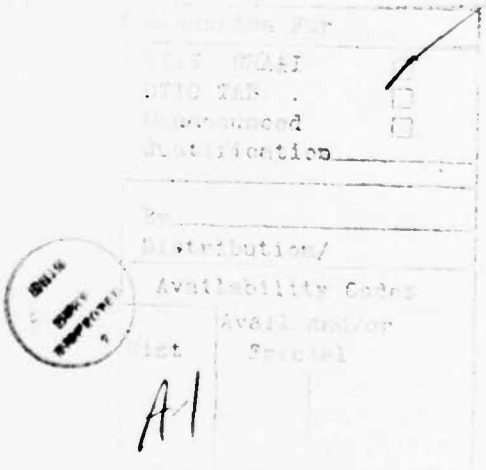

TABLE OF CONTENTS

I. INTRODUCTION

This research is an integrated theoretical and experimental investigation of the nonlinear interactions which may occur between the chemical kinetics, the fluid dynamics and the unstable resonator of a cw fluid flow laser. The objectives of this grant were to measure the frequency and amplitude of the time dependent pulsations in the power spectral output which have been predicted to occur in cw chemical lasers employing unstable resonators to extract power[1,2]. These time dependent fluctuations in cw power, which were shown to be a consequence of rotational nonequilibrium, were shown to occur on lines whose saturated gain zone does not fill the unstable resonator; the amplitude of the fluctuation is determined by the fraction of the resonator filled by the saturated gain zone of the oscillating line, and the frequency of the fluctuation is determined by the geometric outcoupling ratio and the fraction of the resonator that is filled by the saturated gain of the oscillating line[1,2]. Based on these results, the success of the experimental program depended upon the ability to design an unstable resonator in which the saturated gain zone of one or more of the peak power lines does not reach further into the unstable resonator than the center line. The importance of this point is illustrated by a previous experiment[3] which obtained a null result (no oscillations were observed) because the saturated gain zone of the lasing lines filled the resonator. The design of the unstable resonator, thus, depends upon the ability to predict the length of the saturated gain zones for the lasing lines for the laser to be used in the experimental program. To accomplish these objectives, a thorough characterization of the performance of our Helios CL II laser was carried out to verify the computer models used to calculate the saturated gains.

The results for the entire grant are summarized in the following

sections. The development of the MNORO3, MNORO3SR and MNORO3UR cw HF chemical laser models are summarized in Section II. The results of the experimental characterization of the performance of the Helios CL II cw HF chemical laser as a function of cavity losses, pressure and resonator type are summarized in Section III. The very good agreement of the Fabry-Perot, stable resonator and unstable resonator laser models with the data as the cavity losses and pressure change verifies the models. The major result of this research program was the measurement of the amplitude, frequency and Fresnel number dependence of the time-dependent oscillations which occur on lines whose saturated gain does not fill the unstable resonator; the very good agreement with the data of the a priori prediction of these characteristics of the time-dependent oscillations by the MNORO3UR computer model is a stringent test of the model's validity. Based on these results, the cw HF chemical laser models can be used with confidence in designing these devices.

Besides accomplishing the major objective of the research, several other new results were obtained. The first data from a cw laser for a near resonant energy transfer from v=3, J=3, 4 to v=2, J=14 with a subsequent rotational cascade to v=2, J=11 were obtained. In addition, the stable resonator data indicated that the polarization introduced by the Brewster windows affects the power spectral distribution. The comparisons between the model calculations and the data showed that rotational nonequilibrium effects, in particular the power spectral distribution, are affected by the fluid dynamic mixing. Finally, preliminary data with a new He injector indicated that under certain conditions, it was possible to obtain a 60% increase in laser performance.

In Section IV, several suggestions for future work are described.

II. SUMMARY OF THEORETICAL RESULTS

The MNORO[4] rotational nonequilibrium model has been generalized to include rotational nonequilibrium in the HF(0) as well as in the HF(1) and HF(2) levels. With this change, the model predicts the power spectral distribution in the 1→0 vibrational band as well as in the 2→1 band. As described in the yearly progress report[5], this three-level model worked well except for its prediction of the power split between the 1→0 and the 2→1 vibrational bands. This problem was traced to three approximations in the kinetics model which were corrected. These were: (1) the reverse rate for the cold pumping reaction to HF(3) is larger than the forward rate and hence the reverse reaction had to be included in the model; (2) the HF-H_2 VV reaction was treated as a one-way deactivation of the HF; since the reverse rate for this reaction is within a factor of two of the forward rate, it was necessary to include the forward and reverse HF-H_2 VV reactions in the model; (3) the HF-HF VV reactions, which were not necessary in the two-level model, have a significant influence on the power split between vibrational bands and had to be included in the three-level model. With these changes, the three-level MNORO3 model gives the correct power split between vibrational bands. Finally, to obtain agreement with the CL XI total power, it was necessary to include the deactivation of HF by the DF which is formed in the combustor. A comparison of the run times in Table Ia with those in Table VI of Ref. 5 shows that these additions to the kinetics model caused at most a 25% increase in run time. In the CL XI case, if a 10% error in total power is acceptable, the run time can be reduced by 100 sec by neglecting the DF deactivation of HF. The MNORO3 power spectral distribution is compared with the CL XI data in Fig. 1. The excellent agreement with data shown in this figure is also obtained for the Aerospace laser and our CL II laser. The MNORO3 model and its

	CL II RUN 36		CL XI		AEROSPACE LASER	
	MNORO	MNORO3	MNORO	MNORO3	MNORO	MNORO3
Stiffness measure*	4	4	6	5	4	4
Run Time, sec	270	413	457	437	85	181
Steps	3063	2438	5336	3100	1251	1317
Time/step	0.0881	0.169	0.0856	0.141	0.0679	0.137
Stiffness control parameter BKB	0.1	0.1	10.	100.	10.	10.

Table Ia. Comparison of the operating characteristics of the two and three level rotational nonequilibrium models. *The stiffness of the equation system is indicated by the number of decimal places of agreement between $\alpha_{sat} = -(1/2Le)\ \ell n\ r_o r_L$ and the gain on a lasing line. The number in this row is the number of decimal places of exact agreement between α and α_{sat}.

	CL II RUN 36		CL XI		AEROSPACE LASER		
	P_T	P_{10}/P_T	P_T	P_{10}/P_T	P_T	P_{10}/P_T	P_{32}/P_T
Data	36.0	0.471	6.43	0.49	100.0	0.4315	0.0356
Blaze II	39.9	0.514	5.32	0.516	751.0	0.438	
MNORO3	39.25	0.527	4.74	0.523	617.0	0.447	

Table Ib. Comparison of the rotational nonequilibrium model MNORO3 with the rotational equilibrium model Blaze II and with the experimental data.

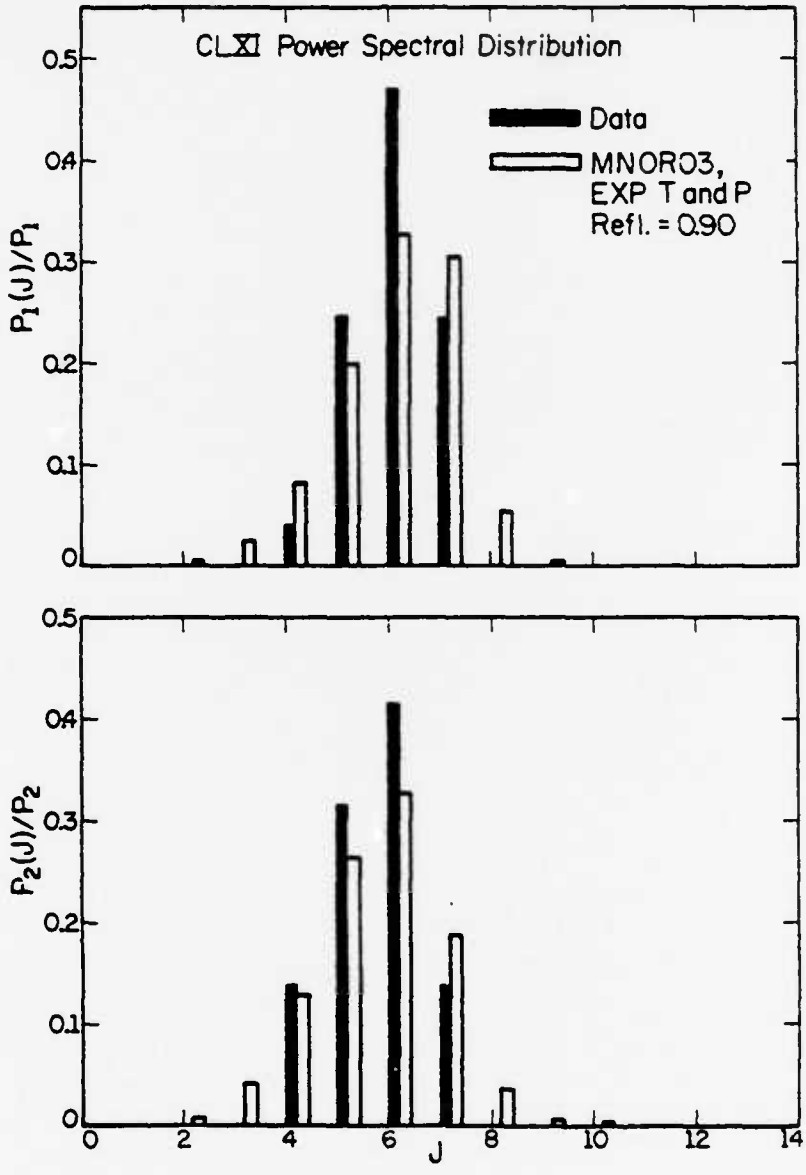

Figure 1. Comparison of MNORO3 Power Spectral Distribution with data for the CLXI.

comparison with the three test cases are described in Ref. 6.

The MNORO3 model has been coupled to a stable resonator model[7]. This code, which is denoted MNORO3SR, has been run for the CL II laser conditions of Run 36 with an x_c of 1.75 mm, which corresponds to the experimentally measured x_c for max power (the H_2 injectors are at $x_c = 0$). The resulting power spectral distribution is compared to the data in Fig. 2. From this comparison it is seen that the extra lines that lase in the Fabry-Perot model do not lase in the stable resonator model and the power spectral distribution is in much better agreement with the data. In fact, for a line to lase in the stable resonator, its gain must be positive on the optical axis and greater than or equal to α_{sat} at some point in the resonator.

However, the theoretical spectra still has too much power in $P_2(6)$ and $P_2(7)$ and not enough in $P_2(8)$ and $P_2(9)$. An examination of the gain distributions indicates that this is caused by the gains on the higher J lines, 8 and 9, not being large enough. Since the relative magnitudes of the gains on various lines is strongly influenced by the mixing, this suggests that the linear scheduled mixing, which was shown to adequately describe the power, power split between vibrational bands and beam diameter as the flow rates and mirror reflectivities were varied[2,8] may not be adequate to give the power spectral distribution. To investigate this question, a study of the effect of nonlinear mixing rates on the power spectral distribution was undertaken. One of the interesting results to come out of this study is the observation that the mixing can make a rotational nonequilibrium spectra look like a rotational equilibrium spectra, that is, only one line lasing at a time in each vibrational band. However, we have never encountered a case where the mixing could make a rotational equilibrium spectra look like a rotational nonequilibrium spectra.

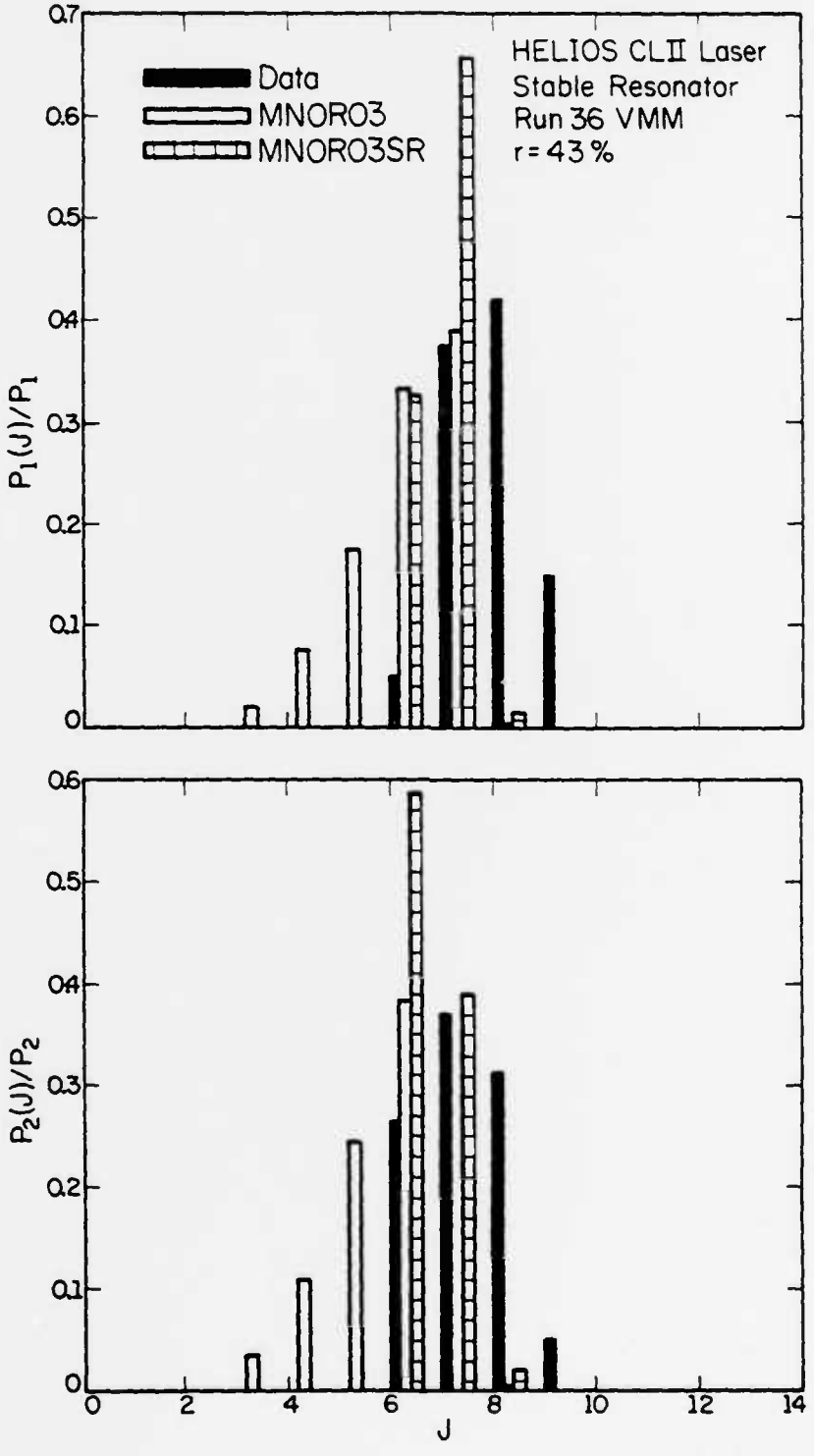

Figure 2. Comparison of MNORO3 + stable resonator (MNORO3SR) power spectral distribution for x_c = 1.75 mm with MNORO3 and data for the Helios CL II laser.

The effect of nonlinear scheduled mixing on the power spectral distribution resulted in good agreement between the stable resonator model and the data, Fig. 3. The nonlinear scheduled mixing shows that the power spectral distribution is significantly affected by the mixing rate. This implies that for situations in which the fluid dynamics of the mixing process are so complicated that they are represented by a very approximate model, the determination of the mixing parameters cannot be considered fixed until a rotational nonequilibrium calculation for the resonator for which the data were taken has shown agreement with the measured spectra.

Although the power spectral distribution for the second nonlinear scheduled mixing case was in good agreement with the data, the power split between vibrational bands was in poor agreement with the data. The power spectral distribution for the first nonlinear scheduled mixing case was not in as good agreement with the data as the second case, but had a better power split. These results suggest that the % SF_6 dissociation may be greater and that the temperature at the H_2 injectors may be less than the values determined from the Fabry-Perot linear mixing calculations[2].

The stable resonator code is implemented in the same way a physical optics-kinetics model[1] is, that is, the code iterates back and forth between the kinetics and the optics. When the code has converged, the total power and the power on each line calculated in the kinetics and the optics parts of the code should be identical and the intensity and the gain distributions on each line should be the same from one iterate to the next. When the present code has converged, all of these criteria are satisfied except for the requirement that the power on each line calculated in the optics and the kinetics must be equal. To date, the reason for this anomaly is not understood. The greatest difference in the power calculated on individual lines in the kinetics and the

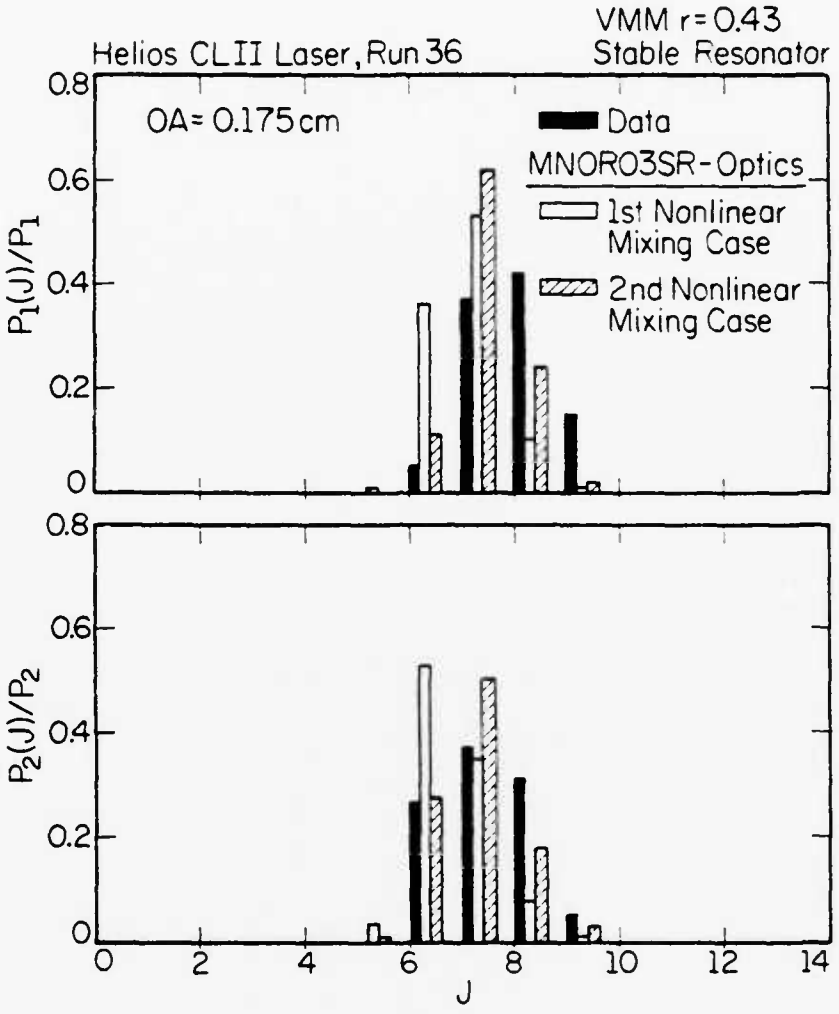

Figure 3. Comparison of the experimental and MNORO3SR first and second nonlinear mixing cases power spectral distributions for the Helios CL II laser for Run 36 at iteration 14.

optics occurs on lines whose saturated gain does not fill the resonator. The larger the fraction of the resonator filled by the saturated gain, the smaller the discrepancy between the power calculated in the optics and the kinetics. The discrepancy varies from 6% for lines whose saturated gain fills 75% of the resonator to 1% for lines whose saturated gain fills 100% of the resonator.

The AFWL wave optics strip resonator model was coupled to the MNORO3 kinetics model to provide a theoretical model, denoted MNORO3UR, for a laser employing an unstable resonator[7]. The seven criteria for convergence are: the change in the total intensity distribution from iterate to iterate, which is calculated in the optics, must be less than some prescribed amount; the changes in the intensity and gain distributions on each line from iterate to iterate must be less than some prescribed amount; the power calculated at the beginning and the end of each iteration must be equal; the power spectral distributions calculated in the kinetics and the optics must be equal; $P_{loss\ total}$ must equal P_{chem}; and $P_{loss\ total}$ and P_{chem} for each line must be equal. All of these criteria were satisfied for the Helios CL II test case (Fresnel number of 1.5).

The study of the Helios CL II laser for Run 36 with a confocal unstable resonator showed that the time-dependent oscillations which may occur on lines whose saturated gain does not fill the resonator are Fresnel number dependent. The time dependent oscillations did not occur for a Fresnel number of 1.5 but did occur for a Fresnel number of 18.57 and for an intermediate Fresnel number of 9.457. For both the large and intermediate Fresnel numbers, the flow conditions had to be altered to stretch the gain zones of the lasing lines. It was shown for the intermediate Fresnel number of 9.457 that, when the standard flow conditions were used, the gain zones were not long enough for any lines to lase. When the flow conditions were altered, the Fresnel number

of 18.57 gave a 10% amplitude variation of the total power and the Fresnel number of 9.457 gave a 15 to 20% amplitude variation of the total power. The intermediate Fresnel number had a larger amplitude variation because the saturated gain filled a smaller fraction of the resonator.

For all cases in which lines oscillated, the period was mostly 6 iterations with some lines varying between 5 and 6 or 6 and 7 iterations[7]. Since the mirror spacing was one meter and each iteration corresponds to one round trip through the resonator, the period was mostly 40 ns with some lines varying between 33 and 40 or 40 and 47 ns.

In July, 1982, Cohen and Bott[9] published the latest recommended HF rate package. Since there are several fundamental differences between the old and the new HF rate packages, a comparative study of laser performance using the old and the new rate packages was undertaken. The case chosen for this study was the CL XI lasing lines experiment which was used as a test case in developing the MNORO and MNORO3 codes. The study was carried out using the Bell Aerospace Textron Blaze II laser simulation code[10]. The approach used was to find a set of reactions whose rates were common to both rate packages for the initial calculation. The various types of reactions were then added to both rate packages, one set at a time. The reactions that were not in the old rate package but were in the new rate package, or vice versa, were added in separately to determine their effect on laser performance.

The comparative study of the performance predicted using the new HF rate package and the old HF rate package showed that the new rate package gives 43% more total power compared to the old rate package, Table II, with over half of this difference in the 2→1 vibrational band[7]. The new rate package gives more total power than the old rate package because there are no multiquantum deactivation reactions by HF and F in the new rate package. The new rate

Table II

Comparison of the old and new rate packages. The HF-DF vv's were added to the new rate package. Both rate packages contain the entire kinetics package. All bands allowed to lase.

	P_{Total} (	P_{10}	P_{21}	P_{32}	P_{43}	P_{54}	P_{65}	P_{76}	P_{87})
		Dimensionless							
		$\frac{P_{10}}{P_T}$	$\frac{P_{21}}{P_T}$	$\frac{P_{32}}{P_T}$	$\frac{P_{43}}{P_T}$	$\frac{P_{54}}{P_T}$	$\frac{P_{65}}{P_T}$	$\frac{P_{76}}{P_T}$	$\frac{P_{87}}{P_T}$
New	8.64	3.76 0.435	4.17 0.483	0.487 0.056	0.0 0.0	0.0 0.0	0.0 0.0	0.158 0.018	0.065 0.007
Old	6.04	3.04 0.503	2.85 0.472	0.147 *0.024*	0.0 *0.0*	0.003 *0.0005*	0.0 *0.0*	0.0 *0.0*	0.0 0.0
Old	5.56	2.77	2.64	0.141	0.0	0.001	0.0	0.0	0.0
Fast HF-H_2 vv		0.499	0.4756	0.0254	0.0	0.0002	0.0	0.0	0.0

	Cutoff 1→0 (cm)	Cutoff 2→1 (cm)	Peak Temp (°K)	$x_{Peak\ T}$ (cm)	Peak Press (Torr)	$x_{Peak\ P}$ (cm)	Peak Velocity ($x10^{-5}$ cm/s)	$x_{Peak\ V}$ (cm)
New	6.03	8.28	506	2.0	18.72	2.00	2.30	10
Old	4.26	4.16	589	2.0	21.85	2.00	2.29	10
Old	3.76	3.73	593	2.0	22.01	2.00	2.29	10
Fast HF-H_2 vv								

package does include the multiquantum deactivation reactions by H but these rate constants are not large enough to decrease the total power. The excess power seen on the 3→2 band for the new rate package results from the absence of the collisional decomposition of HF(3) by H. The single quantum rate was increased for v=3 but not enough to take the place of the collisional decomposition reaction. The removal of power from the upper vibrational bands is accomplished by the single quantum and the DF deactivation reactions in the new rate package, whereas in the old rate package, the removal of power from the upper vibrational bands is accomplished by the collisional decomposition of HF(v), $v \geq 3$ by H atoms[11,6].

The results from the MNORO3 rotational nonequilibrium runs show that the new rate package gives 35% more total power and 30% longer mode width than the old rate package[7]. These differences could be a result of not having the HF-DF vv reactions in the MNORO3 model for the new rate package. However, the spectra given by both rate packages agree well with each other and with the data for the CL XI[7].

With these results for the new rate package, additional runs were made adding in separately the multiquantum deactivation by HF and F and the collisional decomposition reaction for HF(3) from the old rate package. In addition, in the new rate package, the maximum vibrational band for the deactivation reactions was increased to eight to agree with the maximum vibrational level populated by the hot pumping reaction[12]. With these additional reactions in the new rate package, fairly good agreement was achieved with the old rate package, Table III. The total power is now 8.8% lower for the new rate package. There is an even distribution of this difference on both the 1→0 and the 2→1 bands which was not seen before. Although there is a small difference in power on the individual vibrational

Table III

Comparison of the old and new rate packages. The new rate package contains the multiquantum deactivation reactions by HF and F and the collisional decomposition reaction for HF(3) from the old rate package. All bands allowed to lase.

	P_{Total} (	P_{10}	P_{21}	P_{32}	P_{43}	P_{54}	P_{65}	P_{76}	P_{87})
		Dimensionless							
		$\frac{P_{10}}{P_T}$	$\frac{P_{21}}{P_T}$	$\frac{P_{32}}{P_T}$	$\frac{P_{43}}{P_T}$	$\frac{P_{54}}{P_T}$	$\frac{P_{65}}{P_T}$	$\frac{P_{76}}{P_T}$	$\frac{P_{87}}{P_T}$
New (M.Q. only)	6.10	2.81 0.461	2.85 0.467	0.402 0.066	0.0 0.0	0.0 0.0	0.0 0.0	0.0 0.0	0.0 0.0
New (M.Q.+C.D.)	5.51	2.78 0.505	2.60 0.472	0.132 0.024	0.0 0.0	0.0 0.0	0.0 0.0	0.0 0.0	0.0 0.0
Old	6.04	3.04 0.503	2.85 0.472	0.147 0.024	0.0 0.0	0.003 0.0005	0.0 0.0	0.0 0.0	0.0 0.0

	Cutoff $1\rightarrow0$ (cm)	Cutoff $2\rightarrow1$ (cm)	Peak Temp (°K)	$x_{Peak\ T}$ (cm)	Peak Press (Torr)	$x_{Peak\ P}$ (cm)	Peak Velocity ($\times10^{-5}$ cm/s)	$x_{Peak\ V}$ (cm)
New (M.Q. only)	3.83	4.01	525	2.0	19.47	2.0	2.29	10
New (M.Q.+C.D.)	4.01	3.72	539	2.32	19.95	2.0	2.29	10
Old	4.26	4.16	589	2.0	21.85	2.0	2.29	10

bands, the fraction of the power in the individual bands agree very well. The fast deactivation reaction for v=3 and the collisional decomposition reaction for HF(3) together are probably too much for the new rate package. The rate constant for one of these reactions should be decreased to get better agreement for the 3→2 vibrational band.

Since the old rate package was used in baselining the computer simulation of the CL XI nozzle with the trip jets on, the comparison of laser performance using the old and the new rate packages may be clouded by the approximate treatment in the computer model of the mixing enhancement of the trip jets. Their effect was taken into account by a multiplicative factor used to modify the diffusion coefficient. This factor was determined by requiring agreement of the model's prediction of total power and mode length with the experimental measurements of these quantities. For this reason, the computer simulation of the effect of the trip jets on the mixing should be baselined to the CL XI lasing lines data using the new rate package. Once this has been accomplished, it would be possible to draw conclusions concerning the relative merits of the two rate packages for describing laser performance.

This uncertainty in the treatment of the fluid dynamic mixing points out the need for a set of experimental data similar to the CL XI lasing lines experiment for a mixing geometry for which it is possible to a priori calculate the fluid dynamic mixing. This would remove one uncertainty in the model and provide a set of data which could be used to compare the effect of changes in the kinetic rate packages on laser performance.

III. SUMMARY OF EXPERIMENTAL RESULTS

3.1 MULTI-LINE PERFORMANCE OF THE HELIOS CL II LASER

Since a complete description of the multi-line data and the use of the data in baselining the computer models is given in Ref. 2 and 14, only a brief summary of these results will be presented here. The Helios CL II stable resonator multi-line performance with vacuum mirror mounts was measured as a function of the SF_6 and H_2 flow rates. Through comparison of the measured and the predicted power, power split between 2→1 and 1→0, beam diameter, pressure distribution and power spectral distributions, a set of values for the percent SF_6 dissociation in the arc, the initial temperature of the flow at the hydrogen injectors and the mixing lengths for the primary and secondary streams which gives good agreement with the data was determined. The physical description of the mixing which has emerged from this exercise and is supported by visual observation of the flame indicates that the hydrogen jets remain intact with minimal breakup and mixing with the primary stream. The reaction appears to occur on the surface of the hydrogen jets. Because of the similarity between these hydrogen jets and the trip jets used in certain chemical laser nozzles to promote mixing, the present results suggest that the enhanced mixing which results from the trip jets does not result from a break up of those jets but from some other fluid dynamical effect which they induce in the flow[13].

During this modeling exercise, it was found that the rotational non-equilibrium effects, in particular the power spectral distribution, was significantly affected by the mixing rate. This implies that for situations in which the fluid dynamics of the mixing process are so complicated that they are represented by a very approximate model, the determination of the mixing parameters using a rotational equilibrium kinetics model could lead to serious

errors. The mixing parameters cannot be considered fixed until they have been used in a rotational nonequilibrium model and the correct power spectral distribution obtained.

The model was tested by comparing its predictions with the experimental data for different SF_6 and H_2 flow rates. As would be expected, the percent dissociation of the SF_6 and the mixing length changed as the SF_6 flow rate changed. For fixed SF_6 flow rate, the model gave good agreement with the experimental data as the H_2 flow rate changed without requiring any other changes in the input parameters, Table IV.

While the model gives reasonable agreement with the measured power spectral distribution and reproduces the observed shift toward higher J's as the SF_6 flow rate increases, the model generally predicts more lines than are observed. This is a consequence of the Fabry-Perot resonator employed in the calculations. When the calculations were repeated with a stable resonator model which includes the upstream-downstream coupling, the calculated power spectral distributions come into much better agreement with the data, see Section II.

3.2 EFFECT OF MIRROR REFLECTIVITY ON LASER PERFORMANCE

Several months after the data described in Section 3.1 were obtained, it was determined that the reflectivity of the mirror used in those experiments had decreased from 43% to 39%. To further check the model of the CL II laser, its predictions were compared to the data obtained with the 39% mirror and with a new outcoupler of 56% reflectivity. These data were taken using the vacuum mirror mounts. The only input parameter changed for these calculations was the mirror reflectivity. From Fig. 4 it is seen that for all six flow rate combinations, the model and the data are in good agreement as the mirror reflectivity varies. Fig. 4 shows that the general shift in the power

Table IV

Comparison of the Blaze II and MNORO results with the data for the Helios CL II laser with a stable resonator, vacuum mirror mounts and 43% reflective ZnSe outcoupler.

RUN NO.	32	33	34	35	36	37
$\dot{m}_{SF_6}$, gm/sec	1.36	1.01	0.67	1.36	1.01	0.67
$\dot{m}_{H_2}$, gm/sec	0.0375	0.0375	0.0375	0.0545	0.0545	0.0545
P, Torr	12.0	11.0	10.0	12.0	11.0	10.0
% SF_6 Dissoc.	3.3	4.0	4.0	3.3	4.0	4.0
Initial T, °K	500	450	450	500	450	450
H_2 mixing length, cm	3.0	3.5	4.0	3.0	3.5	4.0
P_T, watts						
Data	35.0	32.5	26.0	39.0	36.0	26.0
Blaze II	36.1	32.0	25.4	44.2	39.5	29.4
P_{10}/P_T						
Data	0.475	0.477	0.495	0.491	0.471	0.495
Blaze II	0.537	0.522	0.512	0.523	0.514	0.507
P_{21}, watts						
Data	18.4	17.0	13.1	19.1	19.0	13.1
Blaze II	16.7	15.2	12.4	21.1	19.2	14.5
MNORO	14.8	13.3	10.8	18.9	17.0	12.5
Beam Dia., mm						
Data	2.92	3.03	2.89	2.84	2.86	2.77
Blaze II						
1-0	3.44	3.09	2.88	2.79	2.65	2.31
2-1	2.87	2.75	2.67	2.44	2.40	2.19
MNORO 2-1	2.74	2.70	2.58	2.35	2.32	2.12

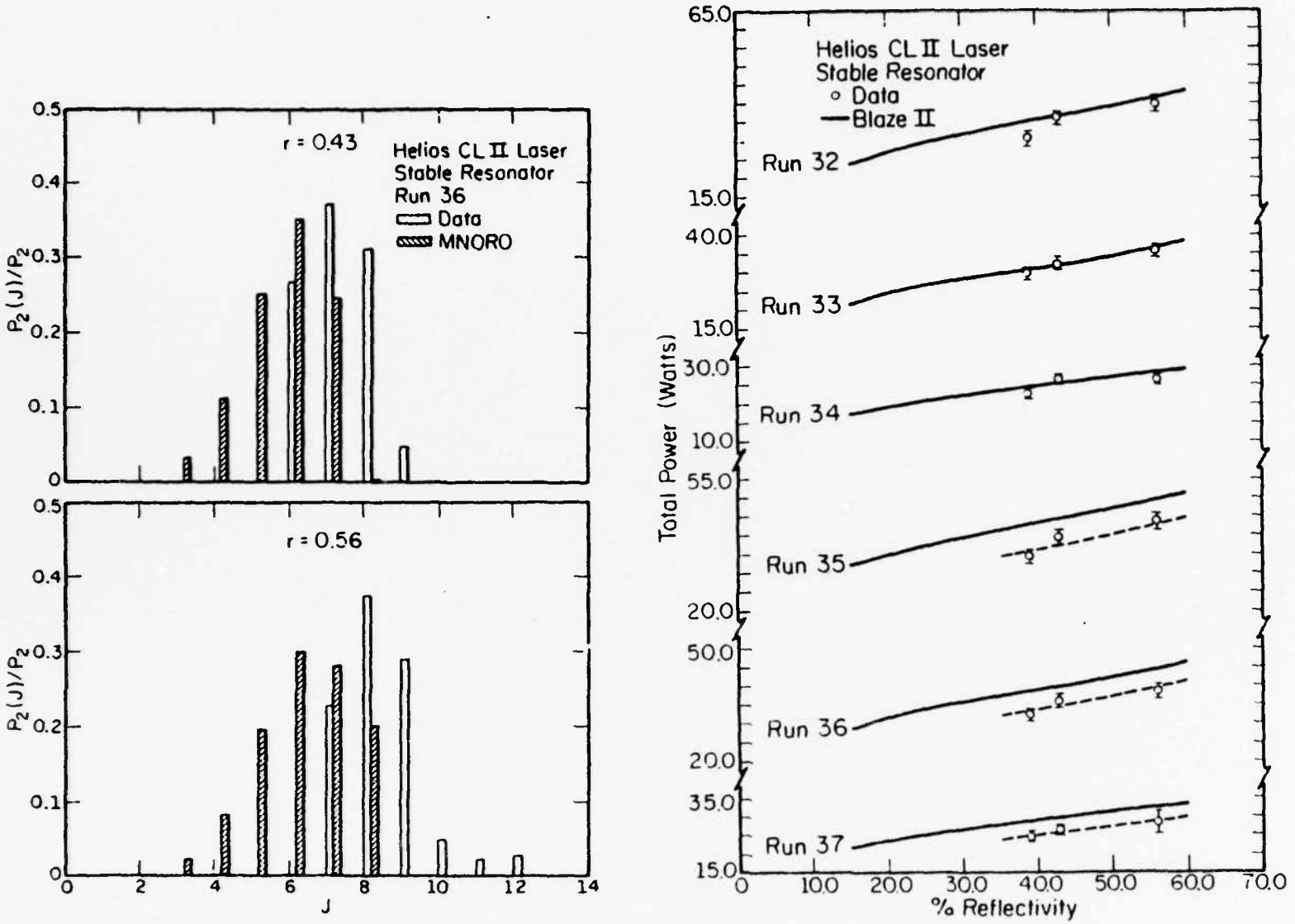

Figure 4. Experimental and predicted performance versus mirror reflectivity for the Helios CL II laser.

spectral distribution toward higher J as the mirror reflectivity increased is reproduced by the model although the model does not quite shift the peak one J higher as occurs in the data.

An unexpected result was the appearance of the lines $P_2(10)$, $P_2(11)$ and $P_2(12)$ with a minimum at $P_2(11)$. These lines were observed for the high and middle SF_6 flow rates for both H_2 flows for the 56% mirror. The corresponding $P_1(J)$ lines observed were J = 7 through 10 with the peak at J = 9. The occurrence of these lines is probably related to the lower losses associated with the 56% reflective outcoupler and the upstream-downstream coupling of the stable resonator. The minimum in the power spectral distribution at $P_2(11)$ may be indicative of a kinetic effect.

3.3 EFFECT OF BREWSTER WINDOWS ON LASER PERFORMANCE

To model the laser's performance when the 4 cm CaF_2 Brewster windows are used, the losses introduced by the Brewster windows must be determined. Since the validity of the CL II computer model as a function of reflectivity was established using vacuum mirror mounts, the losses introduced by the Brewster windows were determined by comparing the measured total power for the six flow rates of SF_6 and H_2 when the 56% mirror was used with the Brewster windows to the P_T versus reflectivity curve predicted by the model. From this comparison, the loss introduced by the Brewster windows was determined to be 17%, Fig. 5, that is, the effective reflectivity with the 56% mirror and the Brewster windows was 39%. To check the determination of the loss introduced by the Brewster windows, the total power was measured for the six SF_6 and H_2 flow rates using the 39% reflective mirror and the Brewster windows. Since the Brewster windows introduce 17% loss, the effective reflectivity ir this case should be 22%. These measurements are compared to the model calculations in Fig. 5. From the agreement between the measured and calculated P_T for the

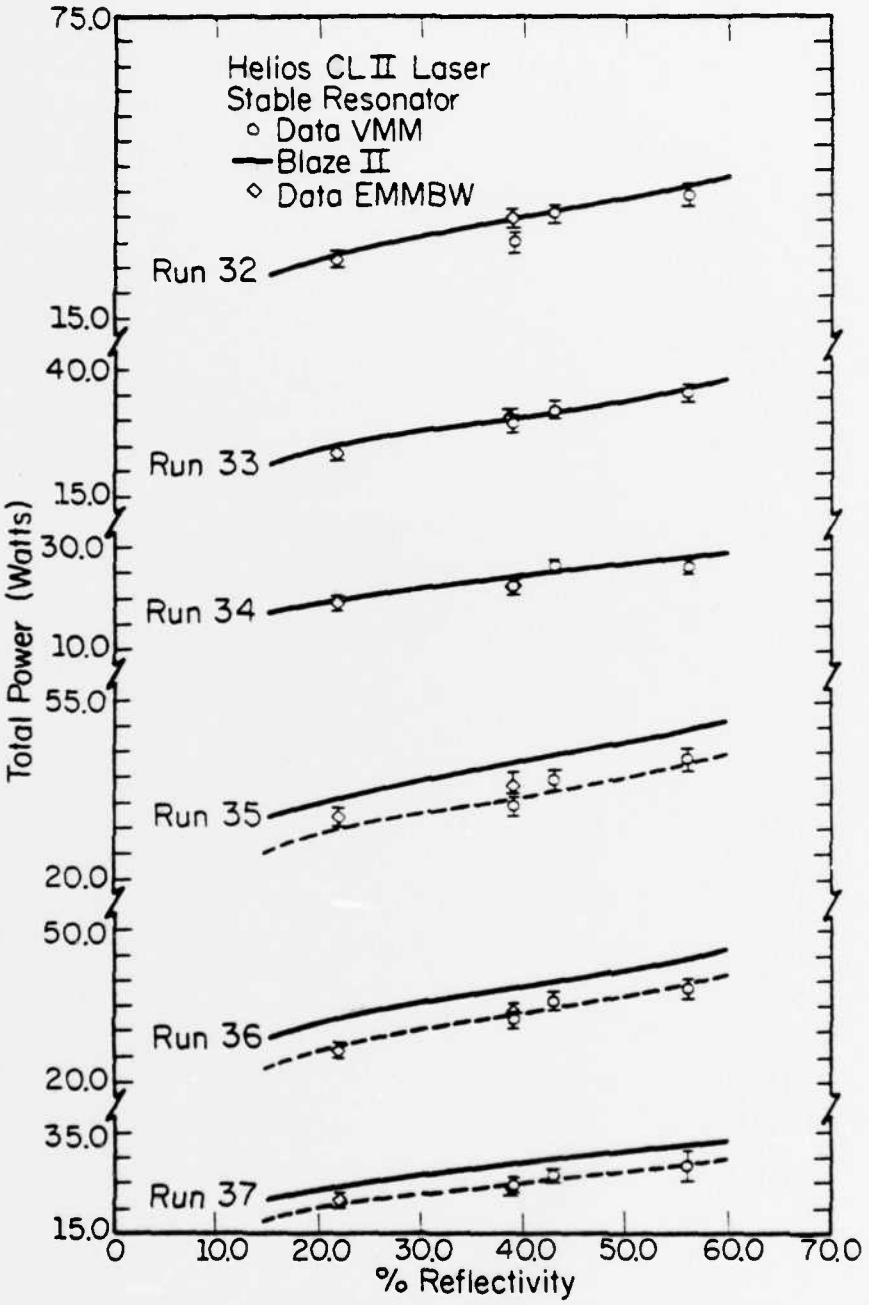

Figure 5. Comparison of experimental and predicted laser performance versus mirror reflectivity for the Helios CL II laser when Brewster windows are used with the 56% and the 39% reflective outcouplers. VMM denotes vacuum mirror mount data; EMMBW denotes external mirror mounts with two Brewster windows data.

39% mirror with the Brewster windows, it can be concluded that the effective loss introduced by the Brewster windows is 17% as deduced from the data for the 56% mirror with the Brewster windows.

The power spectral distributions were measured for all cases except the 39% mirror in vacuum mirror mounts. This data is presented for Run 36 in Table V. Several unexpected effects are apparent. First, as pointed out in Section 3.2, three lines $P_2(10)$-$P_2(12)$ with a minimum at $P_2(11)$ appear when the 56% mirror is used in vacuum mirror mounts, Case 1. As suggested in Section 3.2, these lines are probably a result of the lower losses associated with the 56% mirror. However, when one or two of the Brewster windows are used with the 56% mirror, Cases 3 and 4, it is seen that these same lines occur even though the total losses for these cases are within a couple of percent of the 43% mirror in vacuum mirror mounts, Case 2. When the losses are large enough, Case 6, these lines do not appear. These comparisons suggest that the polarization of the laser introduced by the Brewster windows plays a role in the occurrence of these lines in Cases 3 and 4. In addition to the appearance of these lines in Cases 3 and 4, the polarization appears to suppress lines $P_1(6)$ and $P_2(6)$ in these cases. The results given in Table V are similar to those obtained for the other three flow rate combinations, Runs 32, 33 and 35. A weaker polarization effect is seen in the low SF_6 flow rate cases, Runs 34 and 37. In these cases, the polarization appears to promote the occurrence of lines $P_1(9)$ and $P_2(9)$.

Since the lines $P_2(10)$-$P_2(12)$ are not predicted by the Fabry-Perot model, these cases were studied with the stable resonator model to determine to what extent the occurrence of these lines and the minimum at $P_2(11)$ is a consequence of the upstream-downstream coupling of the stable resonator. The results of this study indicated that the minimum in the spectra at $P_2(11)$ is

Case #	Mirror & windows	r_{effect}	$P_{T,w}$	P_{10}/P_T	BEAM DIA, mm
1	VMM, 56% outcoupler	56%	37.5	0.461	2.83
2	VMM, 43% outcoupler	43%	36.0	0.471	2.86
3	1VMM, 1 Brewster window, 56% outcoupler	41%	34.5	0.503	3.06
4	2 Brewster windows, 56% outcoupler	39%	32.5	0.5[illegible]	3.06
5	VMM, 39% outcoupler	39%	32.5		
6	2 Brewster windows, 39% outcoupler	22%	25.5	0.548	

	$P_v(J)/P_T$										
Case #	$P_1(6)$	$P_1(7)$	$P_1(8)$	$P_1(9)$	$P_1(10)$	$P_2(6)$	$P_2(7)$	$P_2(8)$	$P_2(9)$	$P_2(10)$	$P_2(11)$	$P_2(12)$
1		.0108	.1684	.1929	.0886		.1240	.2019	.1574	.0270	.0129	.0161
2	.0237	.1778	.1987	.0709		.1410	.1964	.1652	.0261			
3		.0321	.1699	.1966	.1039		.0826	.2005	.1467	.0327	.0113	.0237
4		.0994	.227	.1646	.0392	.0007	.1893	.1835	.0919	.0027	.0008	.0006
5		no spectra were taken for this case										
6		.1118	.2665	.1700		.0007	.1836	.2219	.0455			

Table V. Comparison of the experimental data for the flow rates of Run 36[2] for various combinations of mirrors and Brewster windows. VMM denotes vacuum mirror mounts.

not a consequence of the type of resonator used. Thus, this minimum in the spectra at $P_2(11)$ may be evidence for a kinetic effect, namely a near resonant transfer from v=3, J=3, 4 to v=2, J=14 with a subsequent rotational cascade to v=2, J=11, which is the upper level for the $P_2(12)$ line. Since $P_2(12)$ lases, the rotational cascade to v=2, J=10, which is the upper level for the $P_2(11)$ line, is blocked resulting in $P_2(11)$ being weaker than $P_2(12)$.

3.4 EFFECT OF OPTICAL AXIS LOCATION ON STABLE RESONATOR PERFORMANCE

In order to vary the optical axis location for the unstable resonator experiments, the entire invar rod structure which holds the external mirror mounts was mounted on two translation stages. Prior to installing the unstable resonator mirrors, the laser performance as a function of the location of the optical axis of the stable resonator using the 56% reflective outcoupler and the two 4 cm CaF_2 Brewster windows was measured for the six SF_6 and H_2 flow rate combinations. The results are shown in Fig. 6. $x_c = 0$ at the location of the H_2 injectors. From Fig. 6 it is seen that the x_c for maximum power for the low H_2 flow rate occurs 0.25 mm further downstream than for the high H_2 flow rate. This is consistent with the fact that the measured beam diameter is larger for the low H_2 flow rate, Table IV.

3.5 EFFECT OF CAVITY PRESSURE ON STABLE RESONATOR PERFORMANCE

Since the unstable resonator modeling calculations (Section II) indicated that the occurrence of the time-dependent oscillations on lines whose saturated gain does not fill the resonator is Fresnel number dependent and that for the conditions of the high pressure (11 torr) Run 36 that lasing may not occur for a resonator whose Fresnel number is large enough that the time-dependent oscillations should occur, the laser was run at the lowest pressure obtainable in the cavity (about 5 torr) in order to stretch the gain zones. To provide a data base for baselining the computer models, stable resonator

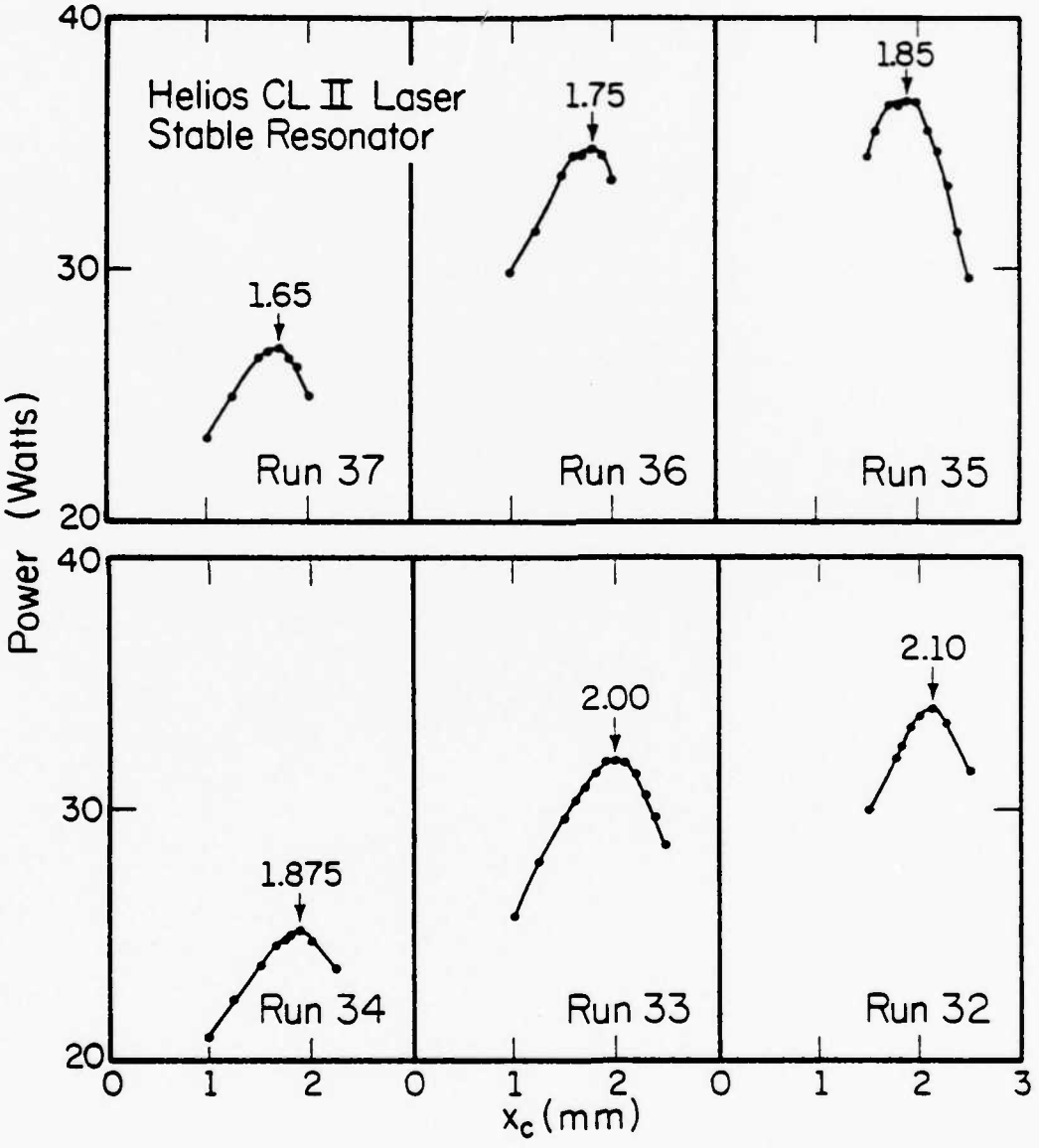

Figure 6. Measured stable resonator power versus x_c for the Helios CL II laser with the 56% reflective outcoupler and two Brewster windows for the six SF_6 and H_2 flow rate combinations. The H_2 injectors are at x_c = 0.0 mm.

power versus x_c was obtained for the six SF_6 and H_2 flow rate combinations with the vacuum control valve wide open. For the x_c of peak power, beam diameters, pressure and spectra were measured. These data were taken with the 56% mirror and two 4 cm CaF_2 Brewster windows, which corresponds to an effective reflectivity of 39%[14]. The Blaze II computer model is compared to the data as a function of cavity pressure in Fig. 7[15]. The only parameter changed in the model for these calculations was the initial pressure at the inlet to the laser cavity. From Fig. 7, it is seen that the model gives very good agreement with the data over the entire pressure range accessible with our vacuum system. Thus, the model agrees with the data as flow rates, cavity losses and pressure are varied. This provides confidence in the model's prediction of the lengths of the saturated gain zones of the lasing lines.

The low pressure data at the x_c for peak power is summarized in Table VI. Since the Run 34 flow rates gave the largest beam diameter, the unstable resonator experiments were performed for this flow rate.

3.6. TIME-DEPENDENT OSCILLATIONS IN AN UNSTABLE RESONATOR

Since the MNORO3UR calculations[7] indicated that the occurrence of the time-dependent oscillations on lines whose saturated gain does not fill the unstable resonator is Fresnel number dependent, the experiments were performed for the flow conditions which gave the longest saturated gain regions. These occurred for the low SF_6 and low H_2 flow rates of Run 34 with the flow control valve wide open, which gave a laser cavity pressure of 5.3 torr. Since the resonator used in the experiments was a 50% geometric outcoupled, symmetric, confocal unstable resonator, the effective size of the concave mirror was twice the size of the hole in the scraper mirror. Since the Fresnel number of the resonator is determined by the size of the concave mirror, the Fresnel number of the resonator was varied by designing the scraper mirror so that the

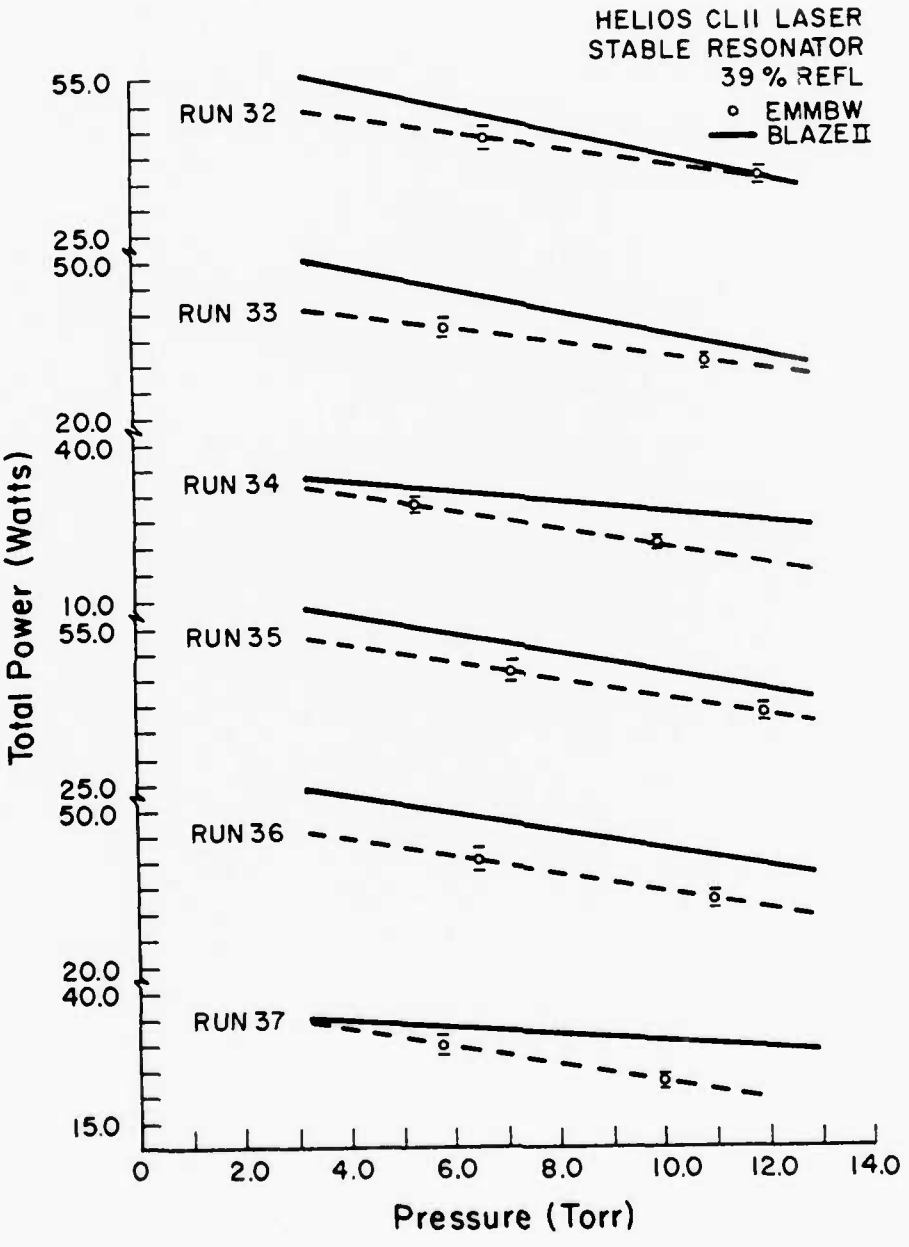

Figure 7. Comparison of experimental and predicted laser performance versus pressure for the Helios CL II laser when Brewster windows are used with the 56% reflective outcoupler. EMMBW denotes external mirror mounts with two Brewster windows data; the effective cavity reflectivity was 39%.

Table VI

Comparison of the Blaze II and MNORO3 results with the data for the Helios CL II laser with a stable resonator with external mirror mounts and 4 cm CaF_2 Brewster windows which result in a 39% effective reflectivity.

RUN NO.	32	33	34	35	36	37
$\dot{m}_{SF_6}$, gm/sec	1.36	1.01	0.67	1.36	1.01	0.67
$\dot{m}_{H_2}$, gm/sec	0.0375	0.0375	0.0375	0.0545	0.0545	0.0545
P, Torr	6.75	6.0	5.40	7.20	6.48	5.83
% SF_6 Dissoc.	3.3	4.0	4.0	3.3	4.0	4.0
Initial T, °K	500	450	450	500	450	450
H_2 mixing length, cm	3.0	3.5	4.0	3.0	3.5	4.0
P_T, watts						
Data	43.7	37.5	28.2	46.2	40.2	29.6
Blaze II	48.5	45.5	31.5	52.6	49.2	33.3
MNORO3		45.9	31.6		49.3	33.6
P_{10}/P_T						
Data	0.481	0.512	0.468	0.493	0.511	0.472
Blaze II	0.504	0.493	0.485	0.501	0.492	0.486
MNORO3		0.504	0.494		0.501	0.493
Beam Dia., mm						
Data	4.90	5.00	5.10	4.60	4.50	4.50
Blaze II	5.30	5.60	5.70	4.10	4.30	4.30
MNORO3		5.50	5.90		4.80	4.70

slit width could be varied from 0 to 1 cm. Because the resonator was symmetric, the distance between the optical axis and the H_2 injectors was equal to the slit width. The layout of the unstable resonator is shown in Fig. 8.

The measurements were made using a room temperature InAs detector. The output beam was chopped with a mechanical chopper. The entire beam was allowed to impinge on the detector to measure the oscillations of the total power. To measure the oscillations on individual lines, the output beam was first passed through a constant efficiency spectrometer, which allowed the output of one line at a time to impinge on the detector. To obtain the period of the oscillations, the output of the detector was displayed on a 500 MHz oscilloscope. To determine the frequency spread of the oscillations, the signal was also displayed on a spectrum analyzer. Since the 500 MHz scope only displayed the A.C. part of the signal, to obtain the amplitude modulation, the signal was displayed on a 100 MHz scope.

Since the complete analysis of the data will be given in Ref. 15, only a summary of the results are presented. The data for the total power for the low SF_6 and H_2 flow rates are shown as a function of Fresnel number in Table VII. The line denoted MNORO3UR is the result of a calculation using the coupled rotational nonequilibrium-wave optics model of our laser[7,15]. This calculation was performed before the experiments to determine whether the oscillations should occur when the optical axis is 5 mm downstream of the H_2 injectors. All of the calculations indicated that the period should be 40 ns independent of the Fresnel number[7,15]. From Table VII, it is seen that in addition to the expected 40 ns oscillation, there was a 7 ns oscillation superimposed on top of it. Since the mirror spacing of the resonator was 1 meter and the round trip transit time is 6.67 ns, the 7 ns oscillation

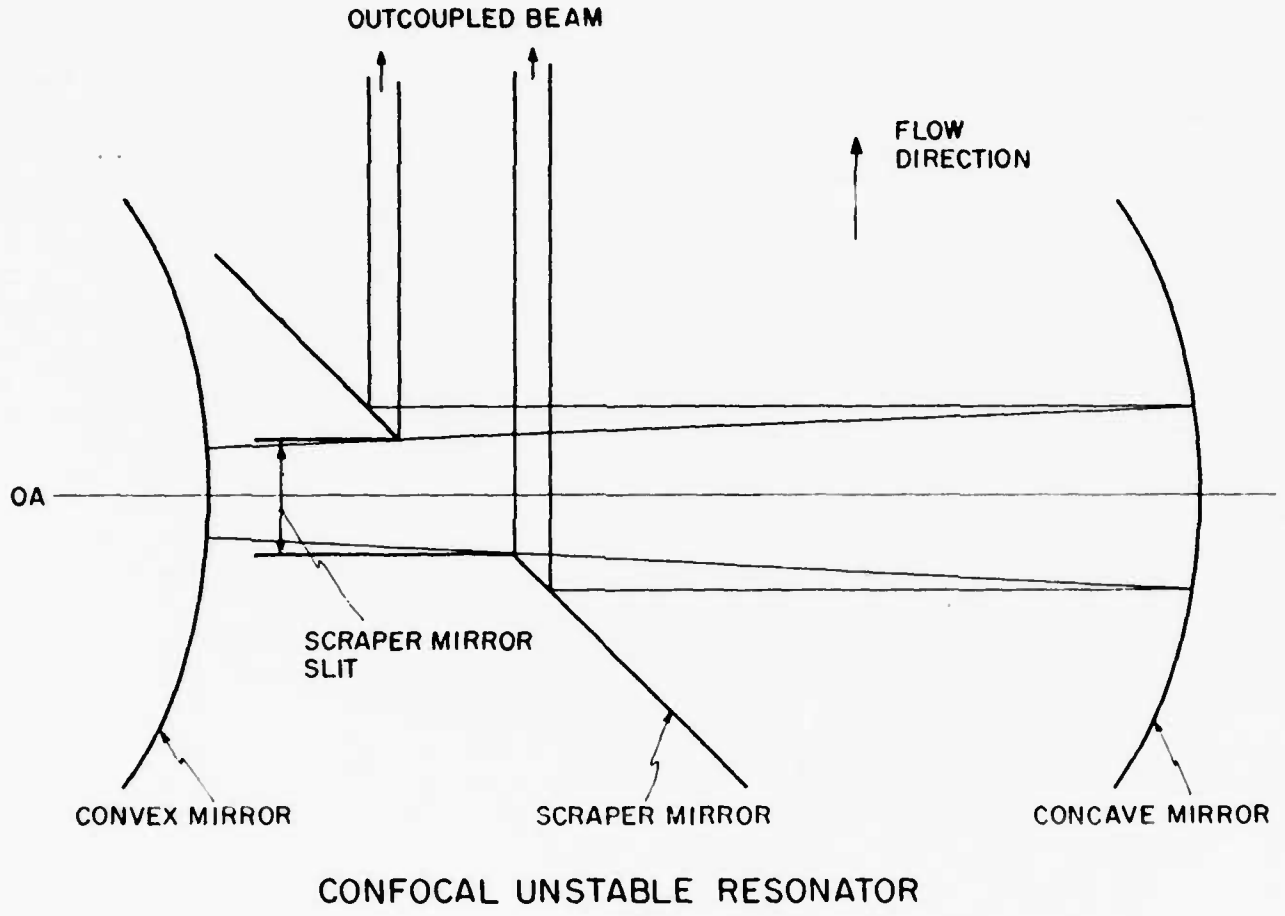

Figure 8. Layout of the unstable resonator used in the measurement of the time-dependent oscillations on lines whose saturated gain does not fill the resonator.

RUN 34 SYMMETRIC CONFOCAL UNSTABLE RESONATOR

SCRAPER MIRROR SLIT, MM	N_F	P_{CAV} TORR	P_T WATTS	OSC PERIOD ns	AMPLITUDE MODULATION $\%P_T$
1.0	0.357	5.31	5.25	7	
2.0	1.428	5.30	5.15	7	
3.0	3.214	5.29	4.10	40/7	3.0
4.0	5.714	5.31	1.90	40/7	22.0
5.0	8.929	5.34	0.70	40/7	25.0
MNORO3UR				40	50.0
6.0	12.857	5.31	0.13	40	50.0

Table VII. Frequency and amplitude of the time-dependent oscillation of total power as a function of Fresnel number for the flow rates of Run 34 at 5.3 torr. The line labeled MNORO3UR is the result of a calculation which was performed before the measurements were made to determine if the time-dependent oscillations should occur when the optical axis is 5 mm downstream of the H_2 injectors.

probably corresponds to a mode beating. Table VII shows that the time-dependent oscillations on lines whose saturated gain does not fill the resonator do not occur for Fresnel numbers below 1.5 and that their amplitudes increase as the fraction of the resonator filled by the oscillating lines decreases. Fig. 9 shows the total power 100 MHz oscilloscope traces for the 4 mm and 2 mm slit widths. Comparison of these traces clearly shows the difference in the traces when the time-dependent oscillations occur.

Table VIII gives the data for individual lines for the 3 mm and 4 mm slit widths. It should be noted that there is a strong cascade coupling between the oscillating 1→0 and 2→1 lines, that is, if $P_2(6)$ oscillates, then $P_1(7)$ also oscillates. From a comparison of the 3 and 4 mm slit cases, it is generally seen that as the fraction of the resonator filled by a line decreases, the amplitude of its oscillation increases. Fig. 10 shows typical oscilloscope traces for an oscillating line.

To provide a qualitative comparison, the theoretical calculations for the 5 mm slit case are shown with the 4 mm slit data. The 5 mm slit calculation is qualitative because the losses introduced by the Brewster windows were not included. In the future, a calculation which includes the effect of the Brewster windows will be performed for the 4 mm slit case. It is seen that there is qualitative agreement between the calculation and the data. The difference in lasing lines between the calculations and the data is due to the omission of the losses introduced by the Brewster windows in the calculation.

To verify experimentally that oscillations on lines whose saturated gain does not fill the unstable resonator do not occur for Fresnel numbers less than 1.5, the x_c of the optical axis was varied from 2 mm to 4 mm for the scraper mirror slit width of 2 mm (Fresnel number of 1.428). No 40 ns oscillations were observed for any optical axis location. The 7 ns

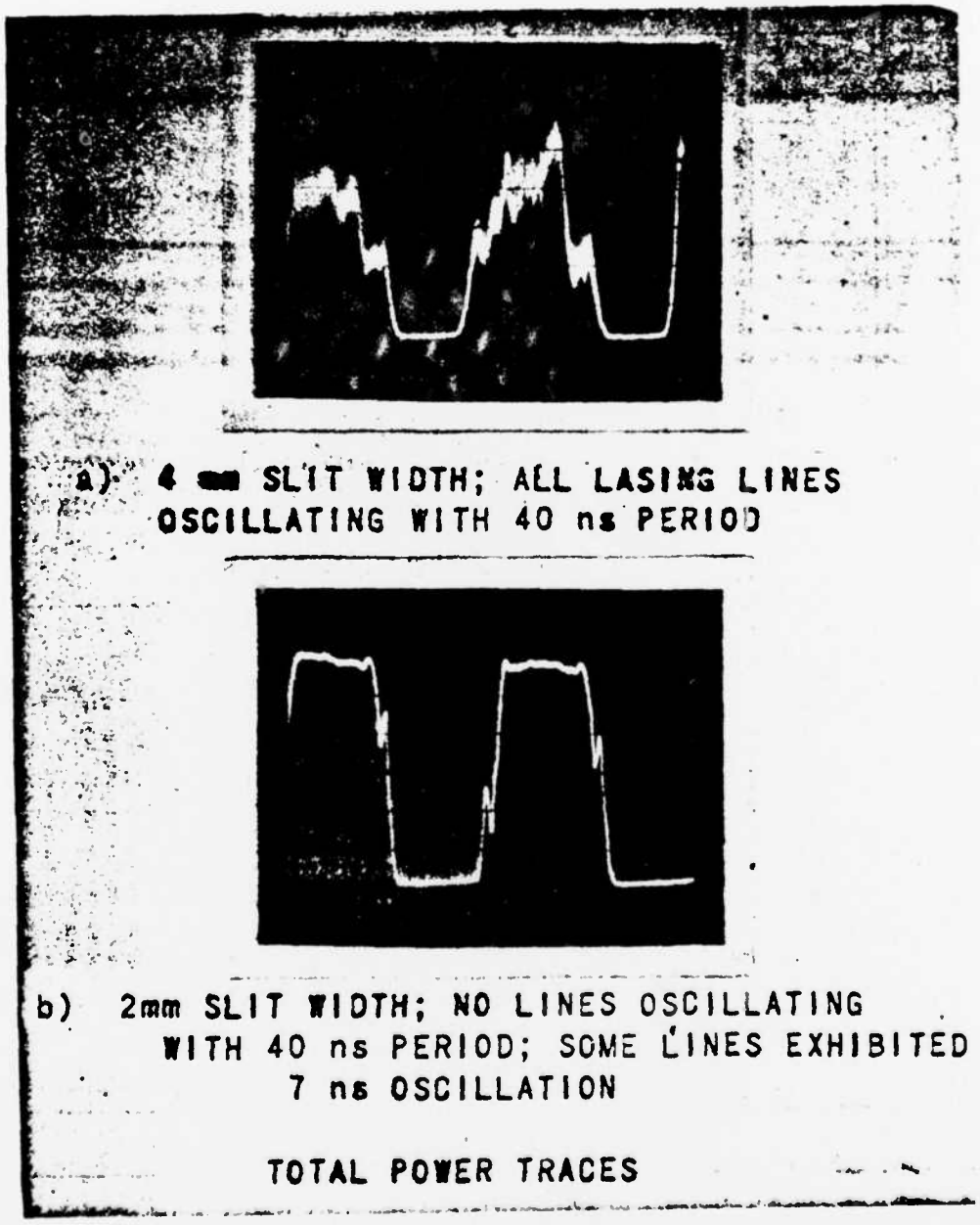

Figure 9. Typical total power oscilloscope traces for Run 34 flow rates at 5.3 torr showing the difference between the oscilloscope traces of an oscillating and a nonoscillating case. For both traces, the scales are 20 mV/div vertically and 0.2 ms/div horizontally.

RUN 34 SYMMETRIC CONFOCAL UNSTABLE RESONATOR

SCRAPER MIRROR SLIT, MM	LASING LINE	$P_1(4)$	$P_1(5)$	$P_1(6)$	$P_1(7)$	$P_1(8)$	$P_1(9)$	$P_2(5)$	$P_2(6)$	$P_2(7)$	$P_2(8)$
3.0	OSC Period, ns			7	40/7	7 weak 40	7		40/7	7 weak 40	7
	OSC Freq., MHz				23-34	23-30			18-29	25-31	
	AMPLITUDE MODULATION $\%P_v(J)$				12.5				20-50	12	12.5
4.0											
	OSC Period, ns DATA				40/7	40/7	weak 40		40	40/7	40/7
	MNORO3UR 5mm Slit	33	40	40	33			33-40	40-47	33	
	OSC Freq., MHz DATA				20-30	20-30	20-30		20-28	18-30	22-30
	MNORO3UR 5 mm Slit	30	25	25	30			25-30	21-25	30	
	AMPLITUDE MODULATION $\%P_v(J)$ DATA				38	80			20-30	66	55
	MNORO3UR 5mm Slit	94	100	75	22.			93	100	30	

Table VIII. Frequency and amplitude of the time-dependent oscillations on individual lines for the flow rates of Run 34 at 5.3 torr for scraper mirror slit widths of 3 mm and 4 mm. The lines labeled MNORO3UR, 5 mm slit are the results of a calculation which was performed before the measurements were made to determine if the time-dependent oscillations should occur when the optical axis is 5mm downstream of the H_2 injectors.

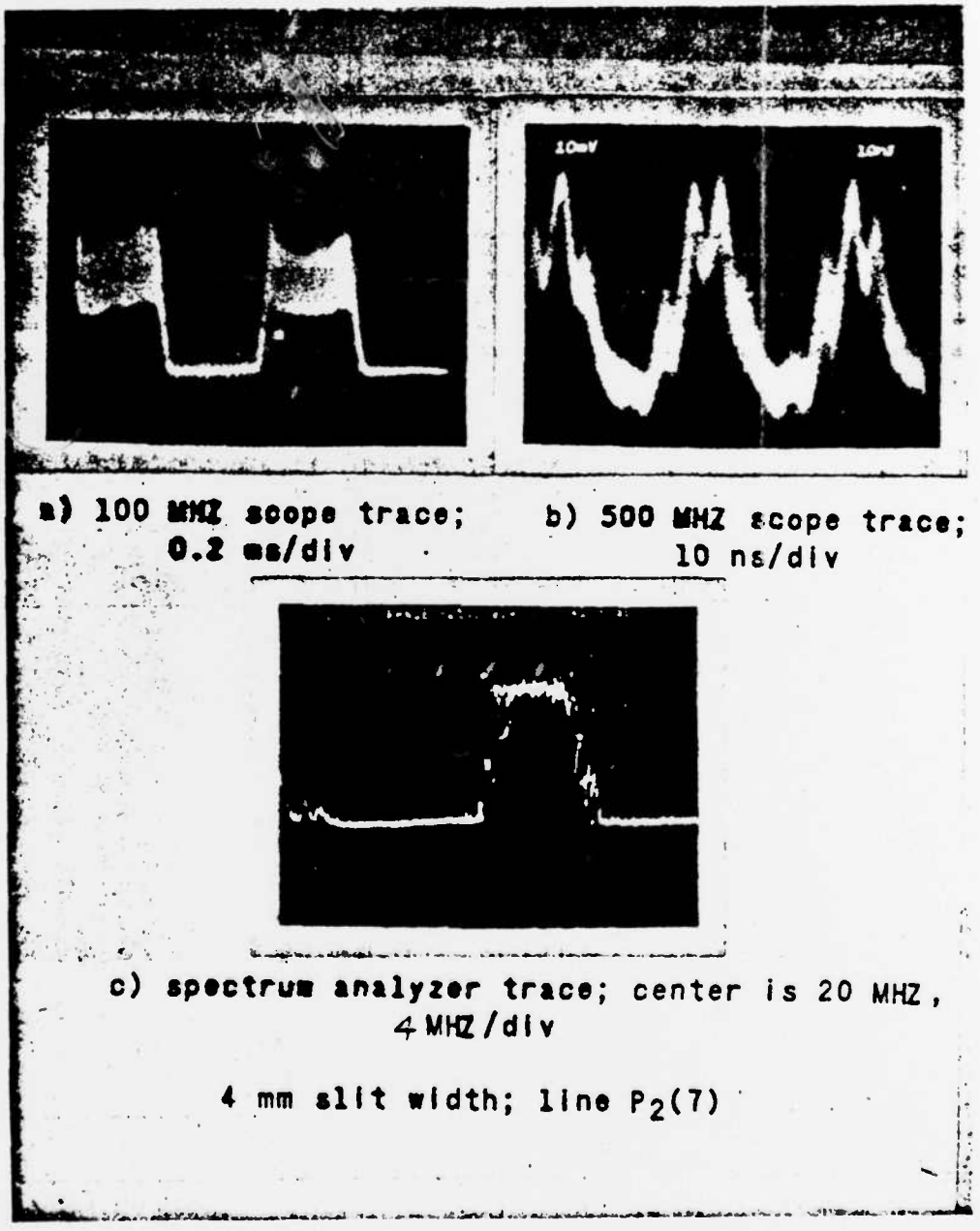

Figure 10. Typical oscilloscope traces of the time-dependent oscillation on a line whose saturated gain does not fill the unstable resonator. This data is for the $P_2(7)$ line for a scraper mirror slit width of 4 mm for the Run 34 flow rates at 5.3 torr. The beam was chopped with a mechanical chopper. The 7 ns oscillation superimposed on the 40 ns oscillation is clearly evident in b.

oscillation was observed on some lines.

From the comparison of the calculation with the data, it is seen that the predicted variations of the time-dependent oscillations on lines whose saturated gain does not fill the resonator with Fresnel number and with fraction of the resonator filled by the oscillating line are in agreement with the data. It remains to change the geometric outcoupling of the resonator to see if the frequency of the oscillation will change as predicted[1,2].

It should be noted that the time-dependent oscillations on lines whose saturated gain does not fill the resonator have also been observed using a scraper mirror with a rectangular hole in it[15]. In this case, the resonator acts as a three dimensional resonator rather than as a strip resonator as is the case when the split scraper mirror is used. Thus, the time-dependent oscillations occur in both two and three dimensional confocal unstable resonators.

By varying the optical axis location of the unstable resonator and noting when various lines begin to exhibit the time-dependent oscillations, it may be possible by comparison with the MNORO3UR gain profiles to determine the extent of the saturated gain zones in the unstable resonator. If this procedure would work, the occurrence of the time-dependent oscillations could be developed into a diagnostic technique for measuring the extent of the saturated gain zones of the lasing lines in the unstable resonator. Such a capability would represent a significant increase in the level of diagnostic detail obtainable from a chemical laser and would greatly increase confidence in design calculations.

3.7 EFFECT OF NEW He INJECTORS ON LASER PERFORMANCE

Dr. Jeffers of Helios provided us with a new design for the He injectors for our laser. As the SF_6, F, and O_2 leave the discharge tubes, the He is

injected from a concentric sonic slit at the exit of the discharge tubes. Thus, with the new injectors, the He does not pass through the arc. The results for various He, O_2, SF_6 and H_2 flow rates (pressures) are given in Table IX. The most striking results are that for the low SF_6 flow rate, the performance increased from 26.5 watts to 36 watts for the same He and O_2 flow rates and to 40 watts when the He flow rate was doubled. For the middle SF_6 flow rate, the power only increased by 3 watts to 41.5 watts. As the SF_6 flow rate was increased to the high value (45 psi of SF_6), there was no increase in power. Thus, with the new He injectors, the maximum power obtained previously at the high SF_6 flow rate was obtained with the low SF_6 flow rate. Further, it was found that when the SF_6 flow rate was reduced by a factor of 1.76 (from 15 to 2 psig), the power only decreased 25% from 40 to 30 watts. Based on our estimates of percent SF_6 dissociation as a function of SF_6 flow rate[2], laser performance ($P_T/\dot{m}_F$) increased from 1266 to 2001. Thus, by injecting the He downstream of the arc discharge, it appears that much more efficient use is made of the SF_6.

There are several possible mechanisms that could be responsible for the increased performance. First, since the He is no longer going through the arc, it is not absorbing any of the discharge energy which would make more of the discharge energy available to dissociate the SF_6. Second, since the He is no longer heated by the arc, the cold He may be lowering the temperature of the flow at the H_2 injectors sufficiently to significantly reduce the deactivation rates of the excited HF, thereby increasing the laser's performance. Third, since the He is injected concentric with the flow exiting the discharge tubes, the cold He may be acting as an insulation layer which inhibits F atom wall recombination and thus more of the F atoms generated in the arc are available for reaction with the H_2. Probably all three of these

CONSOLE SUPPLY PRESSURE, psig							
He	O_2	SF_6	H_2	Power (STANDARD He INJECTORS) watts	$P_T/\dot{m}_F$	Power (NEW He INJECTORS) watts	$P_T/\dot{m}_F$
15	10	15	20	26.5	1266	36.0	1720
35	10	15	20			40.5	
30	10	15	20			40.0	
30	20	15	20			39.5	
30	3	15	20			39.5	
30	10	8	20			35.5	
30	10	2	20			30.0	2001
30	10	8	13			33.5	
30	10	8	15			34.5	
30	10	8	20			35.5	
30	10	8	30			37.5	
30	10	8	23			37.0	
30	10	15	35			42.5	
30	10	30	35			41.5	
30	8	30	35			41.5	
15	10	30	35			37.5	
15	10	30	35	38.0			

Table IX. Helios CL II laser performance with the new He injectors.

effects are occurring. With the data base which has been developed for the laser and the confidence which this has provided in the computer model, it should be possible with a carefully designed set of experiments and modeling calculations to determine the relative contributions of the above mechanisms to the increase in laser performance. The identification of the mechanisms responsible for the improved performance may suggest design changes which would enhance the performance of large scale HF lasers which are of interest to the Air Force.

3.8 CONSTANT EFFICIENCY SPECTROMETER

To obtain the fast response (~ 2ns) from the InAs room temperature detector, it was necessary to hit it with enough power. Since the power which can be allowed to impinge on the grating in the monochromator without causing damage is quite low, a constant efficiency spectrometer based on an idea by Maystre and Petit[16] was designed and tested[17]. This device is based on the constructive-destructive interference which results when a multi-wavelength beam of radiation impinges on a grating oriented so that one surface forming the grooves is parallel to the incident radiation while the other surface, which is perpendicular to the first, acts as a specularly reflecting mirror for the incident radiation, Fig. 11. The mirror and blazed grating are located on radials of a rotating table. The mirror is mounted vertical with the grating tilted back from the vertical at the grating blaze angle α. In this orientation, the large facets of the grating are vertical and the small facets are horizontal. Radiation enters from a fixed point parallel to the rotating table. The input beam strikes the grating first and the wavelength that satisfies the relation

$$\lambda/d = 2 \sin\alpha \cos\phi \qquad (3.8\text{-}1)$$

for the incident angle ϕ has its -1 order diffraction wave behave as though it

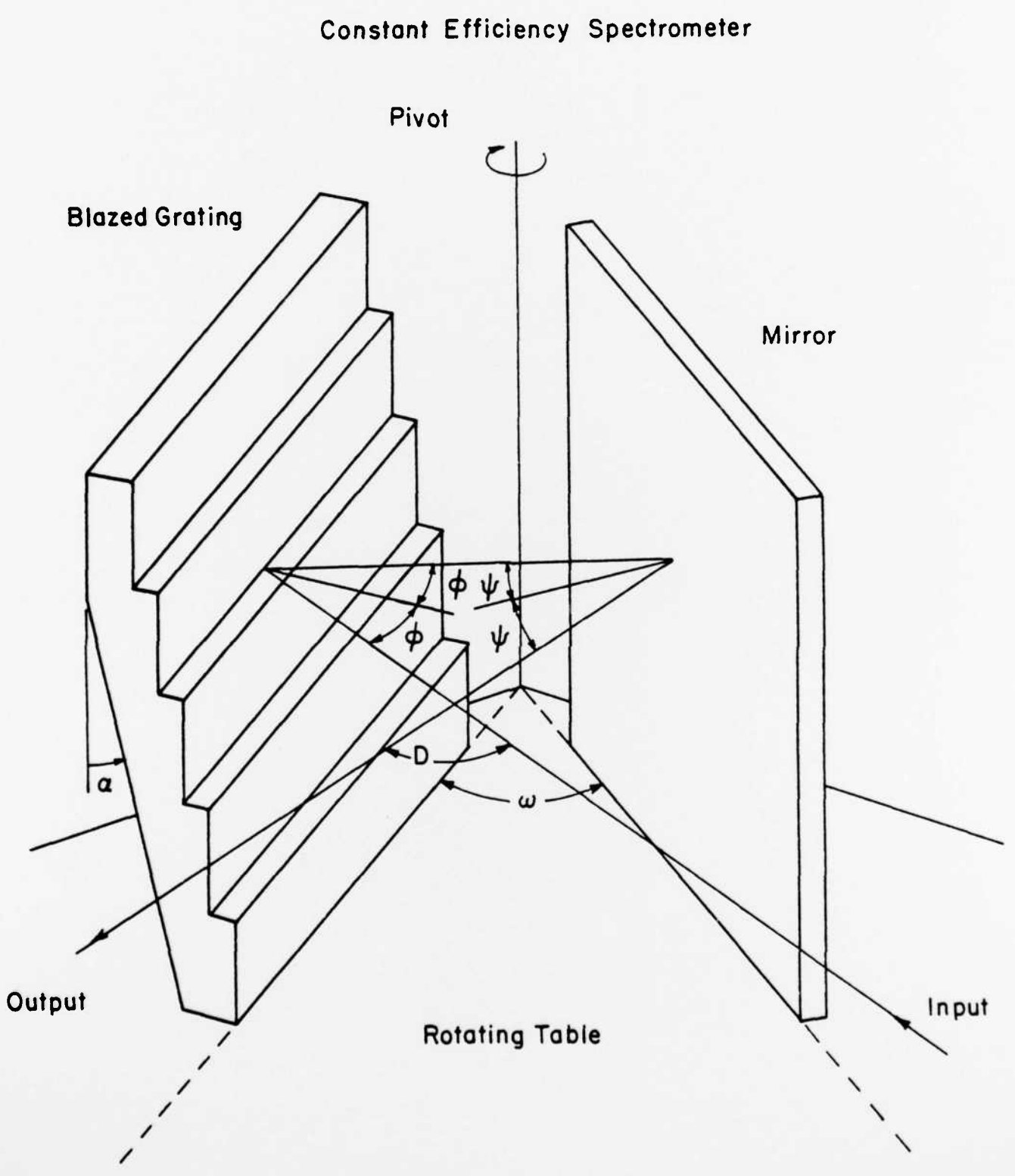

Figure 11. Geometry of the grating and mirror in the constant efficiency spectrometer.

was reflected specularly from the large facets of the grating. For two mirrors separated by a fixed angle ω with the radiation striking each in turn, the net reflected angle Δ is $\Delta = \pi - 2\omega$ independent of the incident angle ϕ. Thus as the table is rotated, each wavelength in turn satisfies (3.8-1) and is reflected out the same exit point.

The grating selected for the spectrometer is a copper original with a gold coating of 98% reflectivity with 300 lines per mm blazed at 27° 45', which corresponds to a reference wavelength of 3.10μ. The mirror is a front surfaced gold mirror of 98% reflectivity. By running the HF laser in the single line mode, the efficiency of the device was measured experimentally as 62.5% independent of wavelength. The wavelength discrimination was measured to be greater than 99% for all wavelengths except the pairs $P_2(7)$, $P_1(10)$ and $P_2(6)$, $P_1(9)$, which are quite close. For the beam diameters used (~ 1mm), 84% to 86% discrimination was obtained for $P_2(6)$, $P_1(9)$ and 32% to 72% discrimination for $P_2(7)$, $P_1(10)$. To achieve discrimination better than 98% for these line pairs would require a beam diameter of 3 mm. While a 3 mm diameter can be approached with the Helios CL II laser for $P_1(9)$ and $P_1(10)$, the stable resonator calculations[7] show that the $P_2(6)$ and $P_2(7)$ lines are significantly less than 3 mm in diameter for the high pressure (10-12 torr) cases.

The constant efficiency spectrometer has been constructed and shown to provide good wavelength discrimination and constant efficiency independent of wavelength. As far as we know, this is the first time such a device has been tested. With the original grating, this device has the advantage of being able to pass large powers and hence can be employed in situations which would damage the usual monochromator.

IV. CONCLUDING REMARKS

The amplitude, frequency and Fresnel number dependence of the time-dependent oscillations which occur on lines whose saturated gain does not fill the unstable resonator have been measured. The good agreement with the data of the a priori prediction of these characteristics of the time-dependent oscillations by the MNORO3UR computer model provides confidence in the model's validity. Based on these results, the rotational nonequilibrium cw HF chemical laser models can be used with confidence in designing these devices.

Besides accomplishing the major objective of the research, several other new results were obtained. The first data from a cw laser for a near resonant energy transfer from a high v, low J to a low v, high J state were obtained. In addition, the stable resonator data indicated that the polarization introduced by the Brewster windows affects the power spectral distribution. The comparisons between the model calculations and the data showed that rotational nonequilibrium effects, in particular the power spectral distribution, are affected by the fluid dynamic mixing. Finally, preliminary data with a new He injector indicated that under certain conditions, it was possible to obtain a 60% increase in laser performance.

The preceding results suggest several additional studies which should be undertaken. The geometric outcoupling of the unstable resonator should be varied to determine if the frequency of the time-dependent oscillations changes as predicted by the calculations[1,2]. Additional data should be acquired and modeling calculations should be performed to determine if the occurrence of these time-dependent oscillations can be used as a diagnostic to measure the length of the saturated gain zones in an unstable resonator. An experiment to verify the hypothesized near resonant energy transfer from v=3, J=4 to v=2, J=14 with a subsequent rotational cascade to v=2, J=11 should be

performed. A series of experiments should be performed to understand the effect polarization has on the power spectral distribution of the laser. A coordinated set of experiments and modeling calculations should be performed to determine the reasons for the increased laser performance produced by the new He injectors.

REFERENCES

1. L. H. Sentman, "Chemical Laser Power Spectral Performance: A Coupled Fluid Dynamic, Kinetic and Physical Optics Model," Applied Optics, 17, 2244 (1978).

2. L. H. Sentman, W. O. Mosebach and P. Renzoni, "A Theoretical and Experimental Study of cw Chemical Laser Performance," AAE 81-8, UILU Eng. 81-0508, University of Illinois, Urbana, IL, December 1981.

3. E. B. Turner, R. A. Chodzko and H. Mirels, "Temporal Stability of Single Line cw HF Chemical Laser with Unstable Resonator," J. of Appl. Phys., 48, 1163 (1977).

4. L. H. Sentman and W. Brandkamp, "An Efficient Rotational Nonequilibrium Model of a cw Chemical Laser," AAE TR 79-5, UILU Eng. 79-0505, University of Illinois, Urbana, IL, July 1979.

5. L. H. Sentman and M. H. Nayfeh, "Nonlinear Interactions Between the Pumping Kinetics, Fluid Dynamics and Optical Resonator of cw Fluid Flow Lasers," AAE 82-1, UILU Eng. 82-0501, Yearly Progress Report AFOSR Grant 80-0133, University of Illinois, Urbana, IL, March 1982.

6. L. H. Sentman and P. Schmidt, "MNORO3: An Efficient Rotational Non-equilibrium cw HF Chemical Laser Model," AAE TR-83-1, UILU Eng. 83-0501, Aeronautical and Astronautical Engineering Department, University of Illinois, Urbana, IL, January 1983.

7. L. H. Sentman, P. F. Schmidt and G. M. Marinos, "Effects of the HF Rate Package and the Optical Resonator on cw HF Chemical Laser Performance," AAE TR 83-6, UILU Eng. 83-0506, Aeronautical and Astronautical Engineering Department, University of Illinois, Urbana, IL, June 1983.

8. L. H. Sentman, M. H. Nayfeh, W. O. Mosebach, P. Renzoni, K. Herrick, K. King, P. Schmidt and S. Townsend, "Theoretical and Experimental Study of cw HF Chemical Laser Performance," Proceedings of the 4th International Symposium on Gas Flow and Chemical Lasers, Stresa, Italy, Sept. 13-17, 1982, Plenum Publishing Corp., NY, in press.

9. N. Cohen and J. F. Bott, "Review of Rate Data for Reactions of Interest to HF and DF Lasers," Report 50-TR-82-86, The Aerospace Corporation, El Segundo, CA, 25 October 1982.

10. J. W. Raymonda, M. Subbiah, J. T. Schimke, S. W. Zelazny and L. H. Sentman, "Advanced HF and DF Chemical Laser Performance Modeling, Vol. 1, The CNCDE/Blaze Rotational Equilibrium Code," T.R. DRCPM-HEL-CR-79-7, Bell Aerospace Textron, Buffalo, NY, 1979.

11. L. H. Sentman, "Rotational Nonequilibrium Effects in cw Chemical Lasers," Journal de Physique, Colloque C9, supplement au n° 11, Tome 41, November 1980, pp. C9-17.

12. N. Cohen, Aerospace Corporation, private communication, February 1983.

13. R. J. Driscol and G. W. Tregay, "Flow Field Experiments on a Tripped DF Chemical Laser," AIAA 14th Fluid and Plasma Dynamics Conference, June 23-25, 1981, Palo Alto, CA, AIAA Paper 81-1271.

14. L. H. Sentman, P. Renzoni, S. Townsend, M. H. Nayfeh and K. K. King, "The Effects of Cavity Losses on the Performance of a Subsonic cw HF Chemical Laser," AAE TR 83-7, UILU Eng. 83-0507, Aeronautical and Astronautical Engineering Dept., University of Illinois, Urbana, IL, June 1983.

15. L. H. Sentman, S. Townsend, G. Tsioulos, J. Bichanich, M. H. Nayfeh and K. K. King, "Time-Dependent Oscillations in a cw HF Chemical Laser Unstable Resonator," in preparation.

16. D. Maystre and R. Petit, "Principe d'un Spectrometre a Reseau a Transmission Constante," Optics Comm, 5, 35 (1972).

17. S. W. Townsend and L. H. Sentman, "Design of a Constant Efficiency Spectrometer for IR Wave Lengths," in preparation.


DATE
ILME